Pertanika J. Sci. & Technol. 32 (5): 1997 - 2011 (2024)

PERTANIKA JOURNALS

SCIENCE & TECHNOLOGY

Journal homepage: http://www.pertanika.upm.edu.my/

Mesh Optimisation for General 3D Printed Objects with Cusp-Height Triangulation Approach

Qais Ahmed Habash[1], Noor Ali Sadek[1], Ahmed Faeq Hussein[1]* and Abbas AlZubaidi[2]

[1]Biomedical Engineering Department, College of Engineering, Al-Nahrain University, Bagdad, 10001, Iraq
[2]University of Saskatchewan, Saskatoon, SK S7N 5A2, Canada

ABSTRACT

3D printing (3DP) is increasingly utilized to achieve quick turnaround on various geometric designs and prototypes, being the growing part of additive manufacturing technology (AMT). The 3DP technique effectively improves the production of complex models in terms of low-cost, time-consuming production, and with less material volume. The key to results optimisation with 3DP is the preparation of the geometry. The following techniques can effectively reduce the required time of the 3D printing process for complex and non-linear CAD files. The fused deposition modelling/fabrication (FDM/FFF) techniques become the first choice in many applications, including biomedical ones. Still, some obstacles exist in the geometry roughness and quality zones. This paper proposes an optimisation method for 3D printed shapes used in biomedical devices and instrumentation by minimising the support structure attached to the model using the FDM technique. In this research, we proposed a method for dynamic compensation against gravity-affected parts extended from the main object's geometry using a forward planar learning (FPL) algorithm to minimise cusp height in 3D printed objects. After the slicing stage, the outcomes proved to be of good quality, optimised the object's surfaces, and minimised the printing time by 32%–38%. The proposed method is promising in defining a better setting for slicing and toolpath for FDM 3D printing. However, this method was not tested on other 3DP methods (Stereolithography (SLA), Selective laser sintering (SLS), and Digital Light Processing (DLP)), as more verification efforts need to be done on these 3D printing processes.

Keywords: 3D printing, 3D policing, cartesian 3DP, cusp-high compensation, fused deposition modelling (FDM), geometric roughness, mesh optimization, stereo-lithography

ARTICLE INFO

Article history:
Received: 02 August 2023
Accepted: 01 February 2024
Published: 08 August 2024

DOI: https://doi.org/10.47836/pjst.32.5.04

E-mail addresses:
Qais.Habash@gmial.com (Qais Ahmed Habash)
Noor.Sadek@gmail.com (Noor Ali Sadek)
sabrean2555@gmail.com (Ahmed Faeq Hussein)
Abbas.ubaidi@gmail.com (Abbas AlZubaidi)
* Corresponding author

ISSN: 0128-7680
e-ISSN: 2231-8526

INTRODUCTION

3D printing (3DP) as part of additive manufacturing (AM) is conveniently used for producing customised objects and applies to a number of general and biomedical applications. Research interest is increasing with the development of printing techniques and materials suitable for particular medical applications (Aimar et al., 2019; Sharaf et al., 2021). The recent developments show that exciting and important advances have already been made in different areas of research, teaching, surgical planning, and prosthetic/medical restoratives. Other applications like personalised drugs and organ printing are at an early stage of development (Bächer et al., 2014).

Recently, most 3D printing technologies have been based on layered manufacturing. One of these techniques is fused deposition modelling or stereolithography. The later technology considered the first attempt appeared in 1981, describing the first functional system for rapid prototyping using photo-based polymers. In this slice-by-slice approach, the effective printing resolution, accuracy, and surface smoothness are highly anisotropic at the initial time of this technology application (Jalil et al., 2017).

It shows a considerable variance in surface quality and textural mapping, visual and haptic, depending on the spatial orientation of the printing process, especially when a larger layer thickness is chosen to save printing time, reduce cost and maximise quality. It is a crucial aspect of biomedical instrumentation technologies (Musialski et al., 2019).

The problem is amplified in the case of fused deposition modelling (FDM), which has become one of the widespread standards in additive manufacturing and rapid prototyping fields. Printing with FDM faces several technical and implementation challenges due to several factors that govern the fabrication and process parameters (e.g., z-axis control, thermal loads and capacity, transition and travelling time).

Generally, in all 3D printers, the optimal quality of the mesh surface is maintained by making the printing axis perpendicular to the surface normal. The relatively high x/y-resolution plus the physical smoothing effect may rise, such as from the melted polymeric filament in FDM-based printers, which may lead to an uncontrolled explosion. As a rule of thumb, the higher staircase artefacts that appear between deposited layers are related to greater surface normal alignment with the (positive or negative) printing direction (Umetani & Schmidt, 2019).

Moreover, by tilting the surface normally towards the negative printing direction ("floating" or "overhang"), auxiliary support structures are generated. It leads to poor printing quality in the surface region that touches the support structures, as shown in Figure 1. Dismissal of this structure may cause extra damage and distortion to the model's surface. Furthermore, many complex objects with many branches and anastomosis are difficult to print with high quality using one global orientation. Such a kind complex object needs excessive support structures, which are adverse to object smoothness and

can damage the surface or even break some parts of the model if removed (Sharaf et al., 2020).

In this paper, we propose an approach to decomposing the input model into a set of parts to overcome the limitations of support structure needs and improve the surface quality in 3D printing. Assuming the printing direction is vertical, each component is oriented to reduce the surface's normal deviation from the horizontal axis.

In this decomposition, more constraints should be taken into account to ensure that the shape of individual pieces remains compact and that the parts can reassemble in order. We initially defined the parts according to the intersection of convex spatial cells with the input model's volume to achieve this.

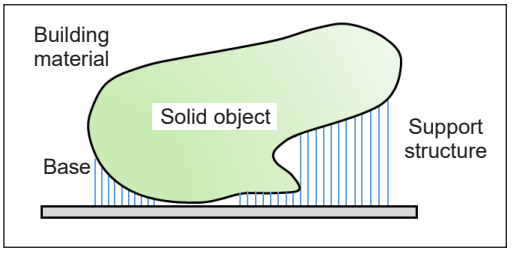

(a)

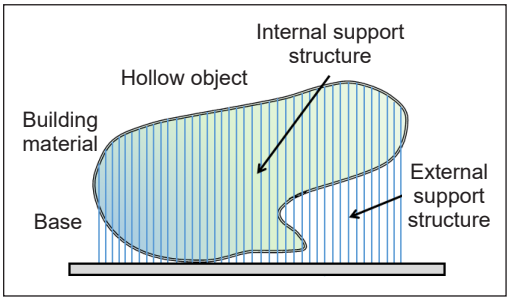

(b)

Figure 1. Schematic of support structure configuration in 3D printing: (a) for a solid object; and (b) for a hollow one

Fused Filament Fabrication (FFF) Method

Consumers love the fused Fabrication (FFF) method since it is cheap and popular compared to SLS and SLA printing methods. The printer head of these machines heats a polymer-based filament until it melts, then deposits the melted filament in predetermined spots that match the model's geometry (Ultraker's RepRap technology) (Sharaf et al., 2020).

Once placed over the layer profile, the molten polymer (semi-liquid) cools and immediately solidifies. The process continued layer by layer until the model's shape was fully formed. The most common material for 3D printing is polylactic acid (PLA), but other thermoplastics, such as acrylamide butadiene styrene (ABS), are also acceptable. The level of detail and features produced by parametric models made using FFF is typically lower than that of models made using other 3D parametric techniques (Yamanaka et al., 2014). In order to prevent the gravity effect and gap-printing defects that can occur with FDM, geometric-support profiles and structures may be necessary, in contrast to SLS and inkjet.

Geometry-related 3D Printing Artifacts Categories

The most common file format used in the 3D printing process is (STL), which has several definitions as abbreviations (e.g. Standard Triangle, Triangulation Language, or Stereo-Lithography). Most Computer-Aided Design/Engineering (CAD/CAE) software allows

users to generate the (STL) file format and export it for the final 3D printing production stage (Wang et al., 2013). However, the generated file may face several hurdles and inconsistencies during production, such as tessellation, refining, vertices computation, and exporting/writing processes.

Therefore, a wide spectrum of geometry correction algorithms was developed to overcome any distortion or deformation in the generated object (Zhu et al., 2017). This paper discussed one effective technique to compensate for geometric distortion occurring during the abovementioned procedures. We focused on vertically aligned surfaces as a treatment spot for the over-hanged shapes (extensions outside z-axis 3D printing) (Zhou et al., 2016).

Some work related to mesh optimisation for 3DP structure focused on reducing gap distance and mesh overlapping errors during the assembly process of the 3D model from printed anatomical structures (e.g., bone fragments) by calculating and analysing detectable boundaries for each contact region in clinical image datasets used to generate the STL medical model.

Supporting Structure in FDM 3D Printing

Based on the geometry characteristics of the printed parts, which can be hollow surfaces or solid entities, the support computation of the hollow surface geometry tends to use only the external support structure and ignore the internal one to minimise the cost and travel pattern complexity of the XYZ-motor driving system and minimise the power consumed by the extruder itself.

This solution is economical for hollow parts because it minimises the total material volume (V_{total}) of the filament used in printing and fabrication time. Therefore, each printed layer contains information on extruded filament (volume, weight and relative length) and travel patterns for shells, walls and top regions in vertically aligned parts. These factors will enhance the overall quality of the 3D-printed shape. Figure 2 demonstrates the cross-sectional Hollow part, while Figure 3 depicts the FDM-based 3D printing processes supported by structure terminology.

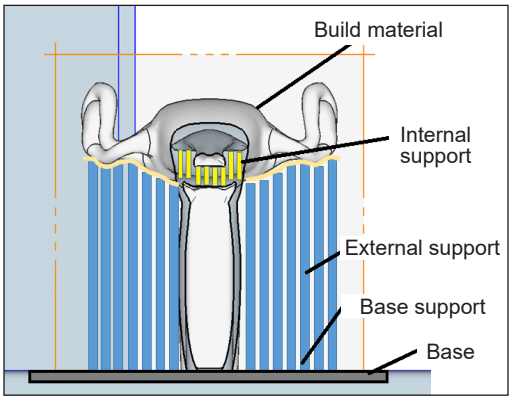

Figure 2. The hollow part cross-sectional view shows external and internal support structures with a printing base

Background and Problem Identification

Regarding the input geometries to 3D printers, there is an understudied issue regarding the design of shapes with less

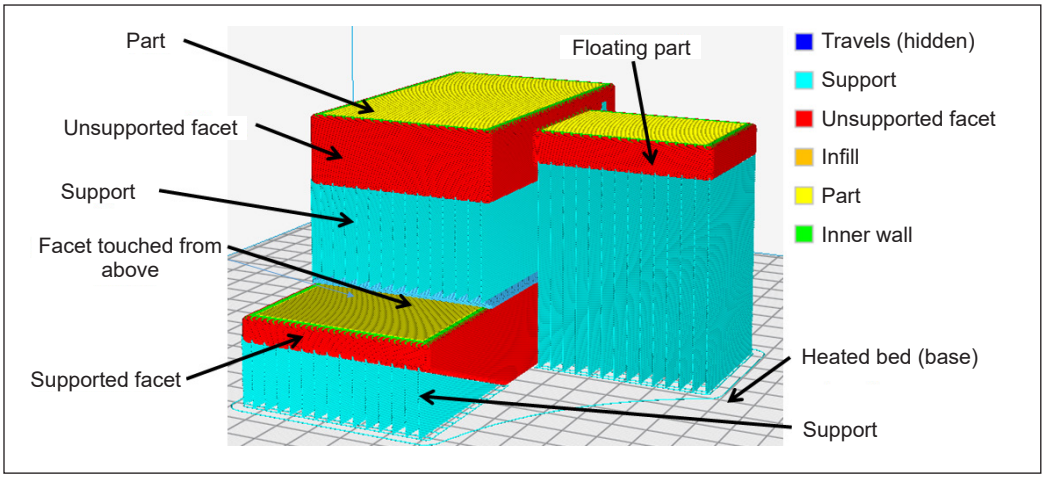

Figure 3. Schematics of the support structure terminology used in the 3D printing process in solid objects with colour-coded territories (blue: travelling direction, magenta: support structure, red: unsupported facets, orange: infill, yellow: parts, green: inner wall region). This coding approach is important to identify the region of geometric processing

support structure models that are more suited for printing, with less roughness in the external layer and walls. A key idea in the FFF method is finding the optimal orientation for the 3D-printed component, and there are a number of ways to handle this aspect of fabrication. Numerous researchers have devised diverse ways for computing optimal orientation, utilising ML algorithms to determine the ideal extruder travel pathway and the most time-effective deposition scenario.

The open-source slicing programme, which prepares the STL file for final printing, already implements many of these methods. Most studies focused on stereolithography (SLS) and stereolithography (SLA) 3D printing processes, although they discovered that FDM and FFF produced superior results.

When it comes to the cost, quality, and integrity of 3D printed components, orientation is typically one of the most important factors among many others. If not, all parameters are included when dealing with general orientation characteristics (GOCs), an error-prone process will be developed by integrating automatic orientation computation in the slicing profile.

We can summarise this characteristic as follows:

- Part's height in the printing direction, which is related to the overall building time and final cost
- Usage of the external support structure, which includes several factors (total volume, entire density and area of contact with 3D printed geometry, inter-support gap distance, and travelling overlapping ratio)
- The quality of faces used in external 3D printed walls (i.e. shells) as its total surface area (TSA) determines the face exposed to the staircase effect.

- Total surface area (SA) of support structure contact with the main shape and also with the base (i.e. heated bed)

Additionally, in addition to the criteria listed above, there are also the considerations of hot-end relative drainage during the printing process (this impact is almost insignificant in tiny nozzle diameters less than 1 mm) and the mechanical strength of the objects that are being built, both of which are not taken into consideration in this optimisation process of the printing process.

The FDM process can have an effect on the computation of GOCs as well as their influence on the final part finishing and cost. For instance, the computation of the FDM support structure considers several elements during the determination process. These considerations include the overall weight of the support structure, the optimal vertical orientation, the base vs the facet supporting profile, surface homogeneity, vertex orientation/angle, and the gravity contact system. Consequently, the computation of the standards will be optimised based on these factors whenever there is a change in the orientation of the 3D product creation process. Therefore, the Cusp-Height Triangulation Approach has been utilised in this work for Mesh Optimisation for General 3D Printed Objects.

MATERIALS AND METHODS

Methodology and Geometry Optimisation for 3D Printed Objects

The staircase effect is the main cause of inaccuracy. Figure 4 depicts the produced vertical and horizontal surfaces (K4 and K1, respectively) that exactly match the proposed models prepared in CAD. However, the process presents some errors according to inaccuracies; they are considered insignificant when compared to errors caused by stair steps (Figure 4). The close horizontal surface (K2) is significantly more affected by inaccuracy than the close vertical surface (K3). For this reason, the facet accuracy should be considered horizontal or

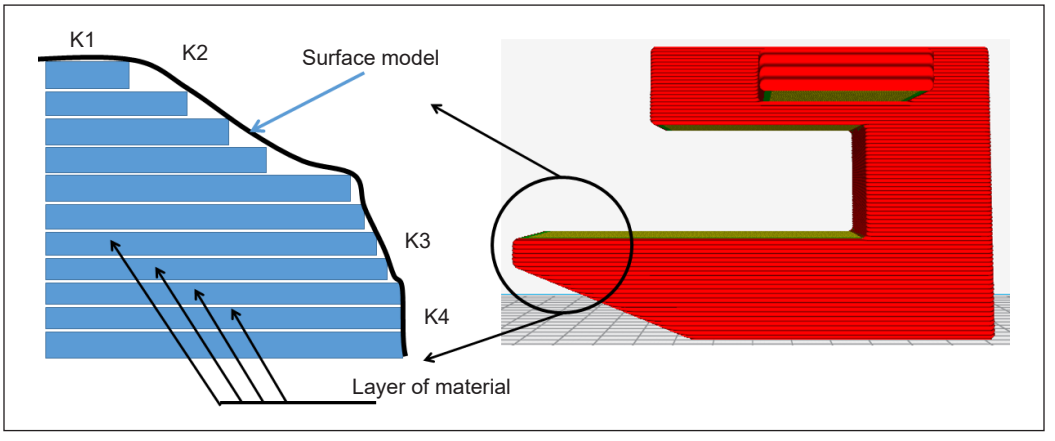

Figure 4. Layer variation in the manufacturing process of 3D printing using FDM technology is due to the staircase effect compared to the real model surface variation

vertical to maximise it, where the "face" entity resembles it over the printing direction. It is not attainable at all times. Therefore, orienting it as close to vertical as possible is desirable.

It is usual for the staircase effect to be the primary cause of surface roughness and loss of fine features in FDM 3D printing. In the worst circumstances, it can also result in the loss of overlapping structure inside the shape (Goh et al., 2022). Therefore, accuracy measurement is done by different researchers (Blumenthal et al., 2013; Jalil et al., 2017). Therefore, many study directions concentrated on digital models in graphical mode, which frequently consist of a large number of triangles. When these triangular edges are immediately mapped to a wire-frame model for 3D printing, the result is complicated structures that directly oppose the goal of a quick production process. Because their definition of the roughness of the CAD model is dependent on the expansion plane (P), which generates an inclination angle that ranges from (90-θ) to the direction of printing, this plane is the one that generates the roughness. An additional parameter that plays a role in the definition of roughness is the maximum distance measured from the surface of the CAD model to the first printable portion (cusp height), also known as (h), because it is significantly dependent on the thickness of the layer and (θ), the angle specified by the cusp-step measure. (Hedges et al., 2012).

The roughness of the local (plane) or surface, sometimes referred to as "cusp height," which is generated from the fabrication of layers during an object's 3D printing process, can be measured by Equation 1:

$$e_\theta = \mid cos(\theta) \mid * h = \mid n^T T \mid * h \qquad [1]$$

where (L) is the thickness of the segmented layer and q is the angle between surface normal n and the direction of printing d, as shown in Figure 5.

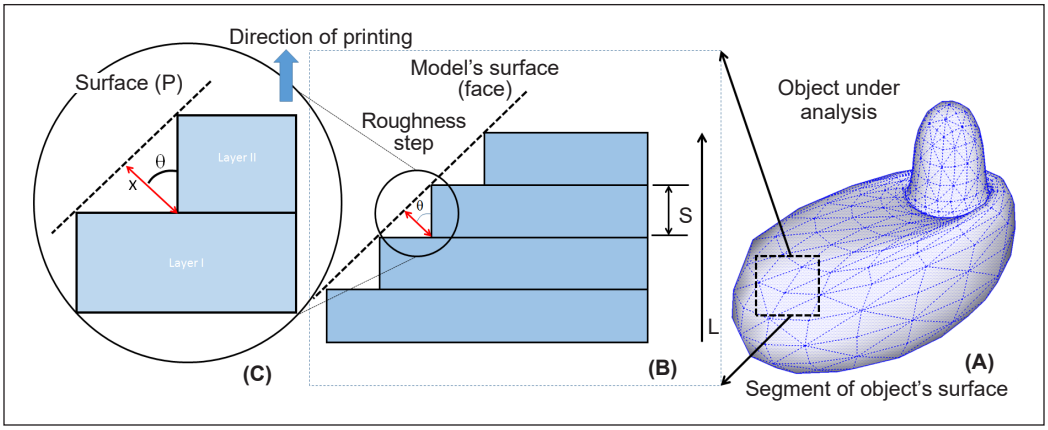

Figure 5. Illustration of Cusp-height error presented in the 3D printed structure (A) the main shape geometry showing the vertices on the surface, (B) the cusp-height error in staircase model of the geometry and (C) Close-up for cusping surface height of the 3D printed object

To guarantee an acceptable quality for the geometry's surface, we require that for each triangle, the angle between surface normal (n) and printing direction (d) lies in some interval $\theta_{neg} < \theta < \theta_{pos}$ with $\theta < 90$ large enough so that the roughness step's height remains small and $\theta_{pos} > 90$ slightly small enough, so no support structures are required in this case.

Therefore, the definition of cusp height is used to measure the shape accuracy and surface quality from the geometry of the part, layer thickness, printing direction, and tolerance of the hot-end nozzle. In light of Equation 1, which applies only in the 2D regime, further modification can be used to apply the same equation in slicing free-form geometries. As many orientations optimisation can be applied in this regime, treating irregular STL faceted shapes could be implemented using the nominal surface interpolation method. This technique is used to minimise energy profiles in facet object-based convex-hull computation.

To clearly approximate the surface optimisation problem, let us consider a single facet present on a surface (S), as depicted in Figure 6. In this approximation, we propose an angle (θ) between the unit vector along the printing direction ($\hat{b}$) and the unit-normal of the surface ($\hat{n}$); hence, the absolute angle value is defined by their dot product, as shown in Equation 2.

$$| cos\theta | = | \hat{b} \cdot \hat{n} | \qquad [2]$$

Triangulating the surface facet allows the accuracy and cusp height to be estimated with Equation 3.

$$h = z_t \, | \hat{b} \cdot \hat{n} | \qquad [3]$$

The 3D object, which composes a higher number of facets as part of the triangulation and meshing process in different directions, may need an adjustable cusp height for higher accuracy. As a result, this compensation mechanism requires comparative weights for all generated facets of the object. A new definition was raised due to this variation in cusp height, and it is called the " influence zone" for the facet's cusp height. This definition is governed by the area (A_{facet}) of the facet itself. It considers the new weighting function relative to other neighbouring facets, as stated in Equation 4.

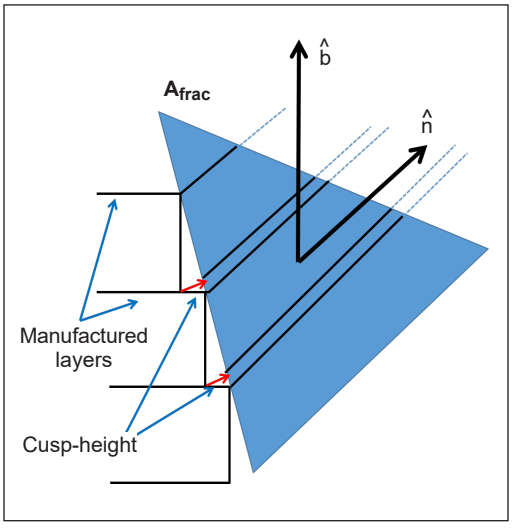

Figure 6. Diagram of STL file accuracy based on one triangular facet approximation

$$h_w = h.A_{facet} \quad [4]$$

Therefore, combining two adjacent facets, even with high-irregular triangulation at their margins, a higher surface area over the cusp height will make the optimisation more influential than a smaller one. We try to "soften" the intersection edges for both facets. This observation iteration can be automated with predictive-surface distortion via (recurrent neural network or tree-model prediction) as this technique is widely used in scaffold quality analysis and validation in tissue engineering applications.

Slicing Implementation

In the process of the part's orientation calculation, the lower facet has a higher cusp height than the large facet, which has a smaller one. It will affect the accuracy of sliced geometry in large surface areas and may generate a wobbling effect in the upward direction. Therefore, slicing implementation for cusp-height (CH) difference correction will be used in the pre-slicing profile for better support structure optimisation in vertically aligned shapes. Therefore, based on the part's accuracy defined in Equation 4, the cusp height computation, which is not sufficient for the total definition of the part's orientation, it is practical to compute the normal of this height variation. Hence, three cases have been defined in slicer software for facets processing in a regular-based model as follows:

- Downward-facing supported facets
- Top-touched facets with supporting skeleton
- Non-supported facets

As a result of this implementation, the inaccuracy in the printed model was reduced to more than 82% based on roughness criteria defined earlier in cusp-height computation, as described in Figure 7. The mesh-optimisation sequence was implemented within the g-code generated during slicing using computed parameters aligned with slice-layer thickness and initial travel time for each layer. This technique will provide more flexibility in the implementation strategy for different iterations in this context.

Segmentation and Mesh Generation

In 3D printed replicas or models, the segmentation is an optional process; however, practically, it is essential in most biomedical and clinical-based applications. The aim of pre- or post-processing is to identify the ROI (region of interest) within an imaging database, which is called segmentation. Besides that, surface extracting from segmented datasets, known as "meshed superficial facet", is another important aim researchers try to achieve.

The thresholding technique permits one to set a series of values from the reserved data while disregarding that drop outside the range. It is an effective and useful tool for retaining or removing regions of interest related to tissue types of density values. Besides,

growing the seed-based region is another segmenting tool. Using this tool, the user chooses zones from the image in simple steps, an initial point or seed, and selects voxel density parameters. The software package then adds extra voxels to the point that agrees with the defined density standards. The added voxels are then added to subsequent adjacent voxels that meet the standards.

When the segmentation is broad, a surface extraction process is started. This management is achieved by extracting the volumetric data by adapting the data from voxel form into a mesh collected faces based on a sequence of triangular facets. It can be accomplished by means of automated rendering tools of surfaces contained within certain software discussed earlier. The conversion from a voxel to a polygonal model, which results in a flatter surface, is an estimate of the original image.

RESULTS AND DISCUSSION

3D Printing Results and Post-processing

Results were obtained by applying the optimisation pipeline for surface roughness reduction and support structure elimination using the forward-adaptive mesh optimisation (MO) algorithm in the slicing software. Results displayed in Figure 8 show a visible reduction of support structure percentage used in the slice-fading profile with open-source slicing software Cura (Ultimaker) and a bold definition of surface roughness reduction due to fine-tuning of layer thickness over a single layer during the 3D printing process shown in Figure 7. In addition, this reduction is even more relevant if we increase the layer heights (initial and standard ones) over the geometric profile in the printing queue. The total iteration presented is averaged for each of the 83 batches in the slicing profile to reach the optimal results with each minimisation percentage, as indicated in Figure 7.

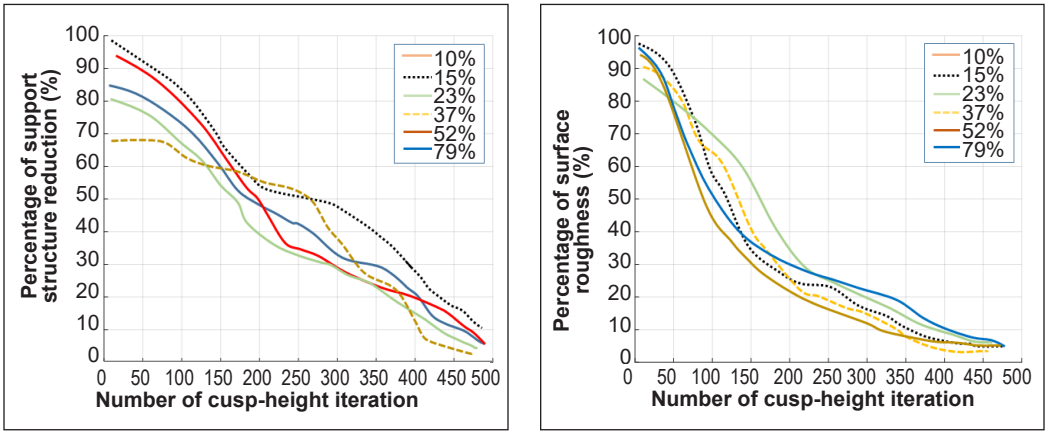

(a) (b)

Figure 7. Optimisation result: (a) Support structure elimination; and (b) geometry's surface roughness reduction with 0.4 mm nozzle hot end setting @ 0.2 mm layer thickness

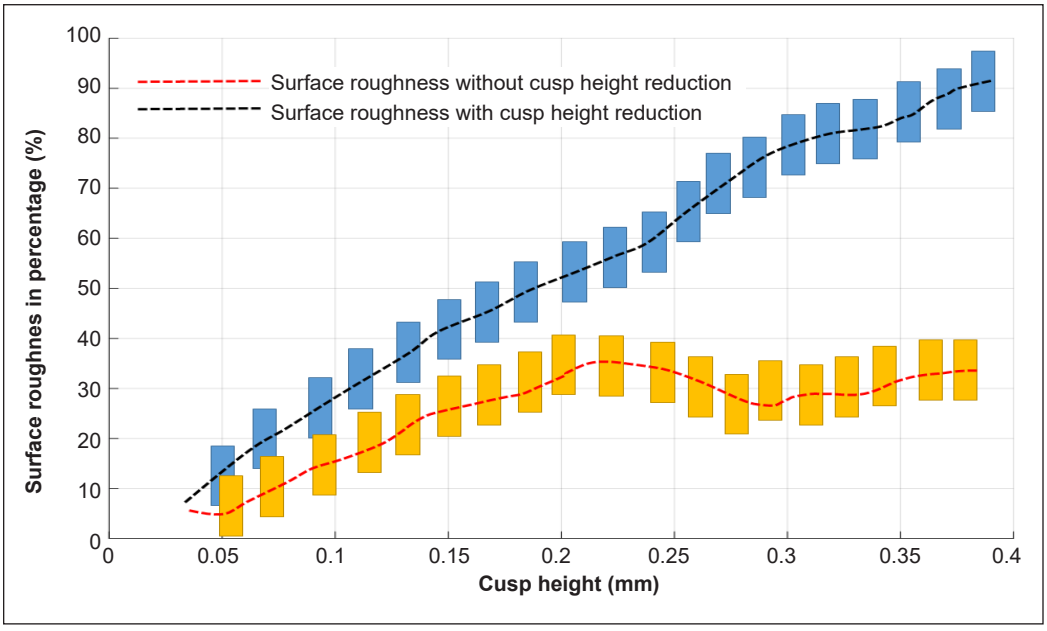

Figure 8. Surface roughness determination for different cusp-height variations with/without CH reduction, as this indicator can be adjusted over the course of printing

Surface roughness is a parameter that represents the average roughness of a surface. It is often used to express surface roughness and the units of measurement for it are either micrometres (μm) or microinches (μin). One of the less prevalent ways to convey roughness is through the proportion of surface roughness present.

With careful examination of the roughness measurement for 3D printed objects, we noticed that with the lower layer height, the lower roughness on the meshed surface, despite the large step size for the cusp-height parameter. It is due to the optimisation level for cusp height (CH) in reference to the layer thickness and invariance of height adjustment during the slicing process. Determination of the relative roughness for performed iteration was measured for each printed sample, as shown in Table 1.

Table 1
Smoothness computation for variable cusp-height versus layer-thickness in FFF 3D printing after using cusp-height (degree) optimisation in slicing profile

Iteration	Layer-height (mm)	Cusp height (mm)	Support (%)	Relative roughness (%)
1	0.175	0.021	11	27
2	0.165	0.025	15	22
3	0.155	0.028	16	19
4	0.145	0.032	19	16
5	0.135	0.035	23	12
6	0.125	0.042	26	10

Moreover, the surface roughness in the case of inclination-based measurement (support structures) may suffer from other tolerance-related values, which may be generated especially in the zones of higher accuracy demands; the sample with specific Y-axis values has a large support area compared to the lower accuracy zone. It is because the sectional computation is performed perpendicularly to the object edge-sand, hence, on or inside a staring step.

For a specific iteration of measuring surface roughness on different 3D printed parts, which is tabulated in Table 2, the value of R*a* with different orientations (0°, 45° and 90°) has been registered with all mean and standard deviations for four different faces of the 3D printed parts produced with the cusp-height optimisation technique.

Table 2
Practical measurement of surface roughness for four printed examples used in this research with combined cusp-height optimisation technique

Printed part	Surface roughness	Inner face				Mean	SD
		Face 1	Face 2	Face3	Face4		
nozzle diameter =0.4 mm with layer height =0.175 mm							
1	Ra@0deg	3.5095	4.1734	0.9037	1.824	2.60	1.50
	Ra@45deg	22.7945	22.4523	24.671	24.0782	23.50	1.05
	Ra@90deg	19.8834	20.4995	23.0288	21.4029	21.20	1.37
nozzle diameter =0.4 mm with layer height =0.185 mm							
2	Ra@0deg	1.7052	6.4298	6.2361	4.6017	4.74	2.19
	Ra@45deg	15.7584	18.5059	14.029	12.0904	15.10	2.72
	Ra@90deg	15.2823	14.4466	17.7571	15.4151	15.72	1.42
nozzle diameter =0.4 mm with layer height =0.2 mm							
3	Ra@0deg	2.0394	2.0662	2.8696	1.2892	2.07	0.65
	Ra@45deg	22.4323	21.8081	20.6335	28.9004	23.44	3.71
	Ra@90deg	21.7547	20.904	19.7598	26.2476	22.17	2.84
nozzle diameter =0.4 mm with layer height =0.22 mm							
4	Ra@0deg	1.4446	1.344	1.6269	0.9773	1.35	0.27
	Ra@45deg	37.0573	36.4608	37.633	36.7085	36.96	0.51
	Ra@90deg	33.2943	32.6814	33.4522	31.7007	32.78	0.79

Limitations and Technical Restrictions

Due to limited FDM-based 3DP technology in the current stage, there is a need for optimal slicing techniques based on machine learning and stepper motor drive and operation over a long period are needed. In addition, to smooth the driving transition, a stable Cartesian movement phasing for the extruder could be implemented to avoid over- or under-extruding for printing samples with large and complex geometric models and parts.

This paper has described a mesh optimisation methodology for a wide range of applications in 3D printing and bioprinting in medicine. Here, we will look at lessons

learned from recent developments and try to make realistic predictions for emerging applications.

As the roughness of 3D printed objects becomes a crucial point in producing high-quality fabricated surgical parts, avoidance of micro-surface scaffolding is important to decrease the opportunities of prosthetic failure and histo-compatibility issues, as many biological 3D printed geometries which possess a high degree of irregularities and non-linearities. It is also true for different shapes printed in various applications. An example of a 3DP shape without/with cusp-height (CH) optimisation approach was demonstrated in Figure 9 for both cases displayed for convenient comparison. As a demonstration of roughness enhancement in 3D printed surfaces, Figure 9 shows different medical parts used in biomedical instrumentation (A-Fan mounting in ventilator systems, Proximal connection in prosthetic hand, B-modular MCU box for Holter cardiac monitor, Brain SpO_2 sensor holder), which can see the effect of CH-optimization algorithm.

Contrary to many researchers focused on different parameters of mesh optimisation, such as minimum length scale and maximum overhang angle, our outcomes support structure elimination with a higher ratio than adjusting chemical additives, which may add extra expenses to the single 3D printing process. However, our method does not cover the non-Newtonian effects on optimal configurations because we focused on solid structure only and not semi-solid or cartilaginous-like materials (i.e. flexible printing material). Mesh optimisation is also in higher demand for 3D bio-printing; it has also facilitated research on early conceptual work for new therapy perspectives, exemplified by the work. Although irregular shapes and geometries associated with these types of bio 3D-printed objects can adversely affect the printing quality, a mesh optimisation technique with cusp height (CH) should be considered in future applications for such fields. In addition, integrating mesh optimisation in microfluidics with 3D bio-printing builds complex co-cultures and tissue structures in test tubes.

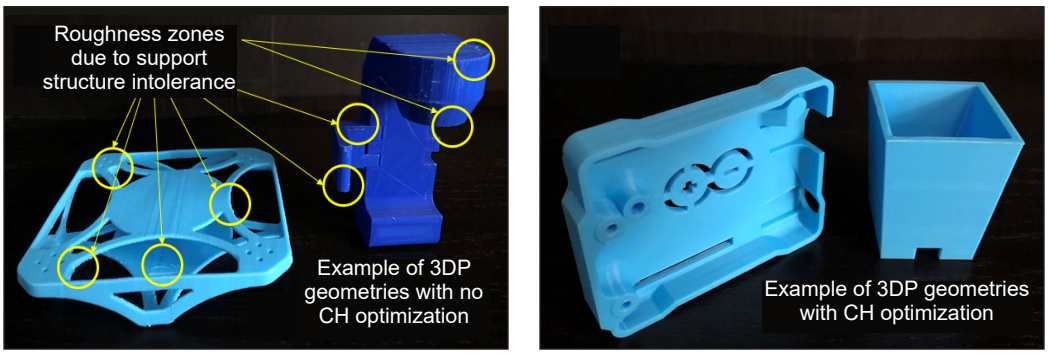

(a) (b)

Figure 9. Examples of 3D printed objects used for validation cusp-height (CH) optimisation technique for minimisation of support structures and lowering roughness percentage of the external wall of shapes: (a) with roughness displayed on parts surface; and (b) with smoothness all over the part surface due to CH utilisation

CONCLUSION

Mesh optimisation in 3D printing research continues its maturity, and its capacity to provide more accurate models in research of different domains, such as the modelling of cancerous lesions, is the subject of increasing research interest. Developments in the direction of cusp-height minimisation to suppress the low-resolution effect of FDM 3D printing will boost the usage of this technology to hydrogel matrices, printing techniques, and better integration with microfluidics are all important steps to move towards obtaining functioning, robust artificial organs by bio-printing. The latest bio-printers can extrude angiogenic microfluidics networks alongside tissue printing.

Our method, as simulated with slicing iteration, proves that it has an advantage over the orthogonal array method developed in terms of parameters optimised, such as print pattern (linear), orientation on the X-axis (0-180°), support angle (45°) and sidewalk (0.175 mm). The slicing profile was implemented to get better surface roughness results and proved to be a smoother transition in support structure utilisation in different segments of 3D printed parts. However, more optimisation is needed in slicing algorithms to deal with other 3D printing technologies, such as the SLA method. The integration of topology-based slicing and segmentation will help smoothen the printing procedure. However, these steps should be accompanied by a better energy-convergent function in terms of minimal failure rate during the deposition phase.

ACKNOWLEDGEMENT

The authors thank Al-Nahrain University, Bagdad, Iraq, for the great support.

REFERENCES

Aimar, A., Palermo, A., & Innocenti, B. (2019). The role of 3D printing in medical applications: A state of the art. *Journal of Healthcare Engineering*, *2019,* Article 5340616. https://doi.org/10.1155/2019/5340616

Bächer, M., Whiting, E., Bickel, B., & Sorkine-Hornung, O. (2014). Spin-it: Optimizing moment of inertia for spinnable objects. *ACM Transactions on Graphics (TOG)*, *33*(4), Article 96. https://doi.org/10.1145/2601097.2601157

Blumenthal, T., Fratello, V., Nino, G., & Ritala, K. (2013). Conformal printing of sensors on 3D and flexible surfaces using aerosol jet deposition. *Nanosensors, Biosensors, and Info-Tech Sensors and Systems, 8691*, 118-126. https://doi.org/10.1117/12.2009278

Goh, G. L., Dikshit, V., Koneru, R., Peh, Z. K., Lu, W., Goh, G. D., & Yeong, W. Y. (2022). Fabrication of design-optimized multifunctional safety cage with conformal circuits for drone using hybrid 3D printing technology. *The International Journal of Advanced Manufacturing Technology, 120*(3), 2573-2586. https://doi.org/10.1007/s00170-022-08831-y

Hedges, M., & Marin, A. B. (2012, March 14-15). *3D aerosol jet® printing-adding electronics functionality to RP/RM*. [Paper presentation]. Fraunhofer Direct Digital Manufacturing Conference (DDMC), Berlin, Germany.

Jalil, N. A. A., Sharaf, H. K., & Salman, S. (2017). A simulation on the effect of ultrasonic vibration on ultrasonic assisted soldering of Cu/SAC305/Cu joint. *Journal of Advanced Research in Applied Mechanics*, *36*(1), 1-9.

Musialski, P., Auzinger, T., Birsak, M., Wimmer, M., & Kobbelt, L. (2015). Reduced-order shape optimization using offset surfaces. *ACM Transaction Graphics*, *34*(4), Article 102. https://doi.org/10.1145/2766955

Sharaf, H. K., Ishak, M. R., Sapuan, S. M., & Yidris, N. (2020a). Conceptual design of the cross-arm for the application in the transmission towers by using TRIZ–morphological chart–ANP methods. *Journal of Materials Research and Technology*, *9*(4), 9182-9188. https://doi.org/10.1016/j.jmrt.2020.05.129

Sharaf, H. K., Salman, S., Abdulateef, M. H., Magizov, R. R., Troitskii, V. I., Mahmoud, Z. H., Mukhutdinov, R. H., & Mohanty, H. (2021). Role of initial stored energy on hydrogen microalloying of ZrCoAl (Nb) bulk metallic glasses. *Applied Physics A, 127*(1), Article 28. https://doi.org/10.1007/s00339-020-04191-0

Umetani, N., & Schmidt, R. (2013). Cross-sectional structural analysis for 3D printing optimization. *SIGGRAPH Asia Technical Briefs*, *2013,* Article 5. https://doi.org/10.1145/2542355.2542361

Wang, W., Wang, T. Y., Yang, Z., Liu, L., Tong, X., Tong, W., Deng, J., Chen, F., & Liu, X. (2013). Cost-effective printing of 3D objects with skin-frame structures. *ACM Transactions on Graphics (TOG)*, *32*(6), Article 177. https://doi.org/10.1145/2508363.2508382

Yamanaka, D., Suzuki, H., & Ohtake, Y. (2014, December 3-6). *Density aware shape modeling to control mass properties of 3D printed objects*. [Paper presentation]. Computer Graphics and Interactive Techniques (SIGGRAPH-ASIA), Shenzen, China.

Zhu, B., Skouras, M., Chen, D., & Matusik, W. (2017). Two-scale topology optimization with microstructures. *ACM Transactions on Graphics (TOG)*, *36*(4), Article 120b. https://doi.org/10.1145/3072959.3095815

Zhou, Y., Kalogerakis, E., Wang, R., & Grosse, I. R. (2016, October). Direct shape optimization for strengthening 3D printable objects. *Computer Graphics Forum, 35*(7), 333-342. https://doi.org/10.1111/cgf.13030